10.2514/6.2024-0689

# Quantifying Secondary Species Emission from Surfaces Bombarded by an Ionic Liquid Ion Source

Christopher T. Lyne*, Miron F. Liu †, and Joshua L. Rovey‡
*University of Illinois Urbana-Champaign, Urbana, IL, 61801*

**Plume-surface interactions are an important field of study for electric propulsion devices of all types. High-energy (keV) plume species impacting a surface can result in many possible interactions, including sputtering, secondary electron emission, and reflection of the incident particle. Plume-surface interactions are especially complex for ionic liquid electrospray plumes, which contain a mixture of molecular ions and ion clusters. A specialized diagnostic known as a "Secondary Species Emission probe" (SSE probe) can be used to quantify the emission of charged secondary species and correct for the associated measurement errors. Here we demonstrate, for the first time, how time-of-flight mass spectra can be corrected for SSE effects and how that correction affects the calculated plume species fractions. Further, we demonstrate how an SSE probe can be used in tandem with an energy analyzer and mass spectrometer to measure the SSE yields of specific species at specific impact energies, providing the first experimental method do to so. Correcting time-of-flight data for SSE effects, we find that the error in plume current density is -10% in the raw measurements. However, SSE correction had a negligible effect on the calculated monomer and dimer fractions. When SSE correction was applied to a time-of-flight dataset representing a narrow range of species energies** $(1772\,V < \phi_{SP} < 1820\,V)$**, we found that the raw (uncorrected) data underestimate the dimer fraction, resulting in a -6% error in the calculated average mass-to-charge and a -14% error in the corresponding mass flux. These two novel applications of SSE measurements have the potential to improve accuracy and reduce uncertainty in measurements of electrospray plume properties and the associated performance estimates.**



## I. Nomenclature

| | | |
|---|---|---|
| $\phi$ | = | electrical potential |
| $\phi_{SP}$ | = | stopping potential |
| $\phi_{RP}$ | = | retarding potential |
| $I_m$ | = | measured current |
| $I_P$ | = | primary species current |
| $I^+_{SSE}$ | = | positive secondary species current |
| $I^-_{SSE}$ | = | negative secondary species current |
| $\gamma^+_{SSE}$ | = | positive secondary species yield |
| $\gamma^-_{SSE}$ | = | negative secondary species yield |
| ToF | = | time-of-flight |
| RP | = | retarding potential |
| SSE | = | secondary species emission |

## II. Introduction

Electrospray propulsion is a type of spacecraft electric propulsion that produces a plume of ions and charged droplets directly from a liquid propellant. The characteristics of that plume depend on the type of electrospray

*Postdoctoral research assistant, Aerospace Engineering, 306 Talbot Laboratory, MC-236, 104 South Wright Street, Urbana, Illinois 61801, and AIAA Student Member. CLyne2@Illinois.edu

†Undergraduate Researcher, Aerospace Engineering, 306 Talbot Laboratory, MC-236, 104 South Wright Street Urbana, Illinois 61801, and AIAA Student Member.

‡Professor, Aerospace Engineering, 306 Talbot Laboratory, MC-236, 104 South Wright Street, Urbana, Illinois 61801, and AIAA Associate Fellow. rovey@Illinois.edu

source, of the propellant, and the operating conditions. One popular approach to find the performance of an electrospray source is to measure the plume properties and use them to estimate thruster performance (e.g., thrust, specific impulse). Most plume diagnostics rely on measuring the flux of charged plume particles to a surface, i.e., they rely on current measurements. However, the measured current includes plume species that impact the surfaces as well as currents associated with secondary species ejected from the surface.

Figure 1 is a drawing of an electrospray source (left) that produces a plume containing molecular ions and clusters of ions. Those plume species are accelerated to energies on the order of keV, resulting in complex collisions with solid surfaces. Those collisions may result in sputtered material, secondary electrons, and rebounding ions or ion fragments, to name a few possible interactions. This phenomenon is known as *secondary species emission* (SSE).

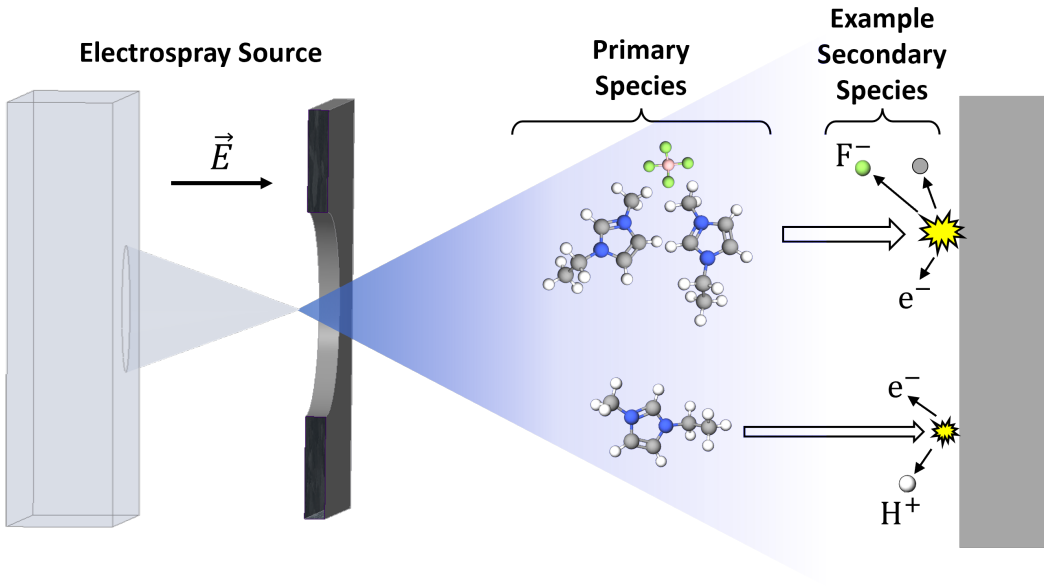


**Fig. 1 An electrospray source (left) emits a plume of ions and ion clusters, which impact the solid surface with kinetic energies on the order of keV. Possible plume-surface interactions include sputtering, electron emission, and backscattering of ions or ion fragments.**

SSE of charged particles cause error in plume current measurements (Figure 2). Furthermore, others have shown that the magnitude of secondary charge emission for surfaces bombarded by ionic liquid electrospray plumes is considerably higher than for traditional xenon-based electric propulsion systems [1–3]. The high secondary species yields imply that SSE is an important source of error for current measurements in electrospray plumes.

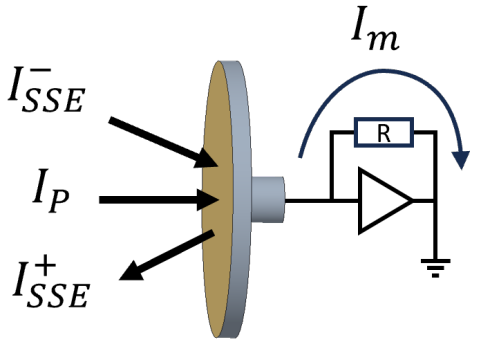


**Fig. 2 Equivalent circuit for primary, secondary, and measured currents. $I_P$ shown pointing towards the collector, implying the primary species are positively charged.**

Secondary species emission of charged particles can be studied using a so-called "SSE probe," which uses a voltage

difference between the current collector and its surroundings to selectively suppress either the positive or negative SSE currents. Figure 3 shows how the suppression of secondary currents can be accomplished by applying a voltage to a grid in front of the grounded collector surface. As explained in the next section, measuring current for the three SSE suppression conditions shown in Figure 3 allows the primary current ($I_P$) and both secondary currents ($I^+_{SSE}$ and $I^-_{SSE}$) to be calculated.

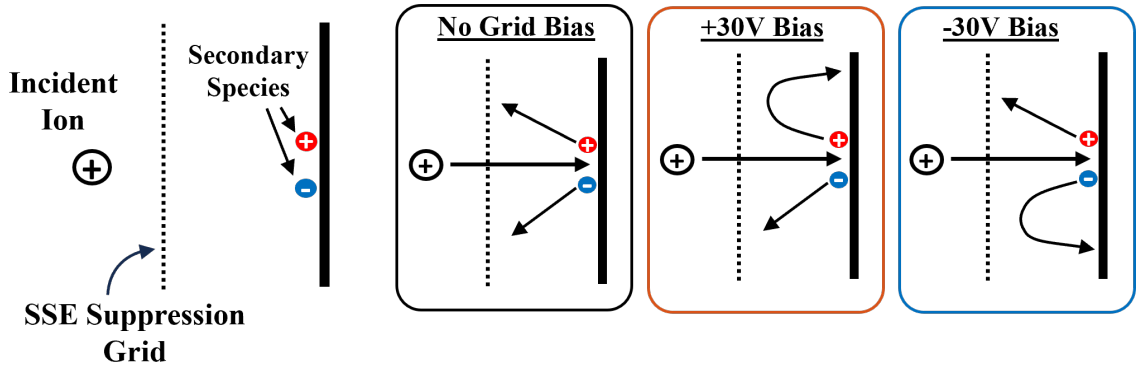


**Fig. 3 Method of selectively suppressing secondary species currents in order to find the primary and secondary currents. The three conditions shown correspond to equations 2, 3, 4.**

Secondary species emission is an important topic in electrospray propulsion besides causing error in plume measurements. For example, SSE contributes to uncertainty in lifetime tests for electrospray devices [4]. Plume species may also contaminate spacecraft components (e.g., sensors), either by sticking to surfaces or otherwise fouling them [cite]. Thus, it is of considerable practical and scientific value to study SSE from surfaces bombarded by electrospray plumes.

In this article, we present secondary charge emission measurements for an ionic liquid electrospray plume impacting a nickel collector plate with an impact energy of 1900 V. The AFET-2 porous electrospray thruster was used as the ion source, operating with the propellant EMI-$BF_4$. We present a new SSE probe design, which we validate by comparing to published values for SSE yield. Next, we present two case studies demonstrating novel applications of SSE probes. The first case study uses an SSE probe in combination with a time-of-flight (ToF) mass spectrometer. The SSE probe is used to calculate the true plume current, removing the error introduced by secondary charge emission from the collector surface. The second case study uses an SSE probe with a tandem energy analyzer / mass spectrometer to measure secondary charge yields for specific species and energies. The data produced by this second method is far more detailed than existing SSE yield data, which generally reports SSE yield averaged over all species and energies present in the plume.

## III. Methods

### A. Measuring Secondary Species Currents

An equivalent circuit for the SSE probe's current collector is shown in Figure 2. The measured current is denoted $I_m$, the primary (incident) current is $I_P$, and the positive and negative secondary species currents are $I^+_{SSE}$ and $I^-_{SSE}$, respectively. The sign conventions associated with each of these currents are also shown in Figure 2. The measured current , $I_m$, is the sum of the primary and secondary currents, as shown in Equation 1.

$$I_m = I_P + I^-_{SSE} - I^+_{SSE} \tag{1}$$

An applied voltage can be used to selectively suppress the secondary currents by pushing positive or negative secondaries back to the collector plate. Three independent measurements can be made, as shown in Figure 3. Equations 2, 3, and 4 give the measured current for the "no suppression", "positive SSE suppression", and "negative SSE suppression," respectively. Those equations can be solved for the three unknowns: $I_p$, $I^+_{SSE}$, and $I^-_{SSE}$. Thus, the primary and secondary currents can be found by making three independent current measurements for three SSE suppression conditions.

$$(I_m)_{No\ Suppression} = I_P + I^-_{SSE} - I^+_{SSE} \tag{2}$$

$$(I_m)_{+Suppress} = I_P + I^-_{SSE} \tag{3}$$

$$(I_m)_{-Suppress} = I_P - I^+_{SSE} \tag{4}$$

Dropping the $m$ subscript on the measured current and rearranging those equations to solve for the primary and secondary currents results in equations 5, 6, and 7.

$$I_P = I_{+Suppress} + I_{-Suppress} - I_{No\ Suppression} \tag{5}$$

$$I^+_{SSE} = I_{+Suppress} - I_{No\ Suppression} \tag{6}$$

$$I^-_{SSE} = I_{No\ Suppression} - I_{-Suppress} \tag{7}$$

The positive and negative secondary charge yields are defined in Equation 8 and 9, respectively. Note that the secondary currents ($I^+_{SSE}$ and $I^-_{SSE}$) will always be positive because secondary species are emitted from the collector surface. A negative secondary species current is not physically meaningful in this context. Thus, the absolute value of primary current ($|I_p|$) is used in Equations 8 and 9 in order to report non-negative yield values for negative primary currents. For example, an EMI-$BF_4$ ion source emitting negative species will impact the collector and the secondary currents will be positive ($I^+_{SSE} > 0$ and $I^-_{SSE} > 0$). By convention (e.g., [1]), reported yield values are positive regardless of the polarity of the incident species.

$$\gamma^+_{SSE} = \frac{I^+_{SSE}}{|I_P|} \tag{8}$$

$$\gamma^-_{SSE} = \frac{I^-_{SSE}}{|I_P|} \tag{9}$$

### B. SSE Probe

Figure 4 shows a cutaway diagram of the secondary species emission probe used in this study. The probe has a similar design to that reported by Uchizono et al. [2]. Both probes suppress secondary species emission by applying a potential difference between the collector surface and the surroundings. In the case of Uchizono et al., they use a grounded shell enclosing the current collector. The grounded shell has an aperture that allows plume species to enter the probe. Secondaries are suppressed by applying a potential to the collector, thus creating an electric field that pulls secondary species of the desired polarity back to the collector. The probe used in this study (Figure 4) instead creates that potential difference by keeping the collector grounded and applying a potential to a secondary species suppression grid in front of the collector surface. Functionally, there is little difference between the approaches—each simply creates a potential difference to 'pull' secondaries back to the collector plate. However, keeping the collector plate grounded simplifies the measurement electronics. Specifically, the transimpedance amplifier, which converts the collector current to a measurable voltage, cannot be easily biased more than 1 or 2 volts with respect to ground.

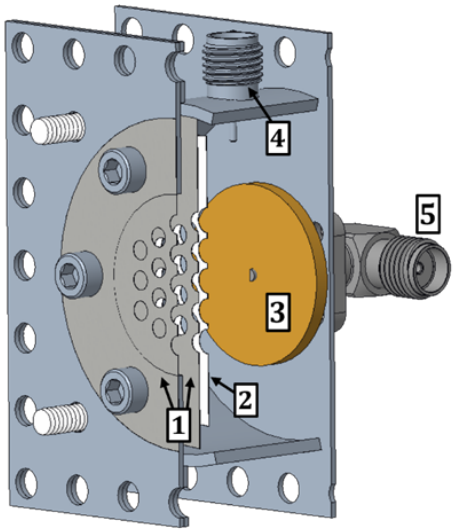


**Fig. 4 Secondary species emission (SSE) probe for measuring secondary charge emission from surfaces bombarded by electrospray plumes. (1) Grounded front grids, (2) SSE suppression grid, (3) current collector, (4) coaxial connector for SSE suppression voltage, (5) coaxial connector for collector current signal.**

### C. Electrospray Source

The electrospray source used in this study is modeled after the AFET-2 porous electrospray thruster shown in Figure 5. The thruster consists of a 24 by 24 grid of electrospray emitters arranged in a grid. Each emitter is aligned with a hole in the extractor grid, allowing an ion beam to pass through. The left side of Figure 5 shows the housing of the AFET thruster, which is electrically connected to the extractor electrode and is grounded. High voltage is applied to the emitter electrode using a threaded connection in the backside of the thruster housing (Figure 5 right). During thruster assembly, the extractor is aligned with the emitter array with the help of an optical microscope.

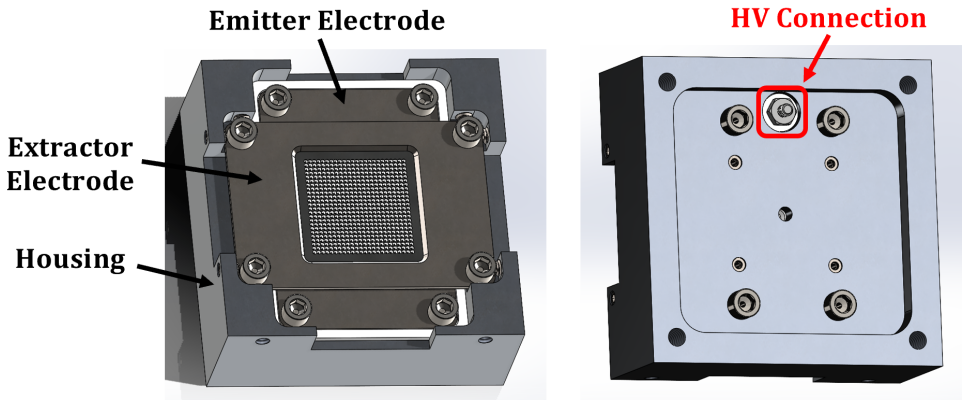


**Fig. 5 CAD model of the AFET-2 porous electrospray thruster. The thruster consists of a 24 by 24 grid of emitters for a total of 576.**

The thruster emitters were made from a P5 porous glass disc with a pore size ranging from 1 µm to 1.6 1 µm. Emitters were machined using a grinding wheel (see [5]), resulting in a four-sided pyramid shape for each emitter. The left side of Figure 6 shows a height map of a subset of emitters measured using an optical profilometer. Each emitter is approximately 250 µm tall, has a half-angle of 15°, and has a radius of curvature of about 30 µm at the tip. The emitters have a tip-to-tip spacing of approximately 550 µm. The gap between the emitter tips and the extractor face is about 200 µm. The right side of Figure 6 shows an image of several emitters taken using an optical microscope.

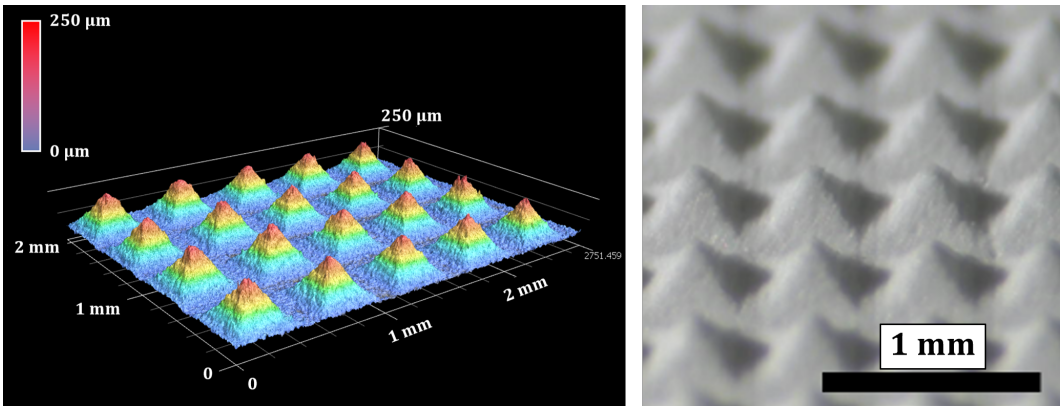


**Fig. 6 (Left) Height map of the AFET emitters measured using an optical profilometer. (Right) Closeup image of several emitters. Both figures reproduced from [5].**



## IV. Results

### A. SSE Probe Measurements

The secondary species emission probe shown in Figure 4 was used to study the interaction of an EMI-$BF_4$ ion beam with a Nickel collector plate. Figure 7 shows the characteristic 's-curve' measured for an impact potential of +1.9 kV. The SSE grid voltage was swept between -30 V and +30 V and the collector current was measured for each grid voltage. The measured currents from Equations 1 through 9 are annotated on the left side of Figure 7. The *saturation currents*, $(I_m)_{+Suppress}$ and $(I_m)_{-Suppress}$, are measured at the largest applied grid voltages. They correspond to the *complete* suppression of positive and negative secondary species, respectively. Using the values shown in the left side of Figure 7 with Equations 8 and 9, the measured charge yields for a +1.9 kV EMI-$BF_4$ ILIS plume on a nickel surface were $\gamma^+_{SSE} = 0.20$ and $\gamma^-_{SSE} = 0.05$.

Klosterman et al. reported secondary charge yields for an EMI-$BF_4$ ILIS plume on several materials at a range of impact energies [1]. After discussing with the authors of that manuscript, it is evident that the positive and negative yield values they reported are reversed. That is, their reported values for $\gamma^+_{SSE}$ are actually the values for $\gamma^-_{SSE}$ and vice-versa. Correcting that mistake, the secondary charge yields they report for a positive EMI-$BF_4$ plume at +1.9 kV are $\gamma^+_{SSE} = 0.2$ and $\gamma^-_{SSE} = 0.1$. Those reported values closely match the yields measured here, lending credibility to the probe design and the data reported in Figure 7.

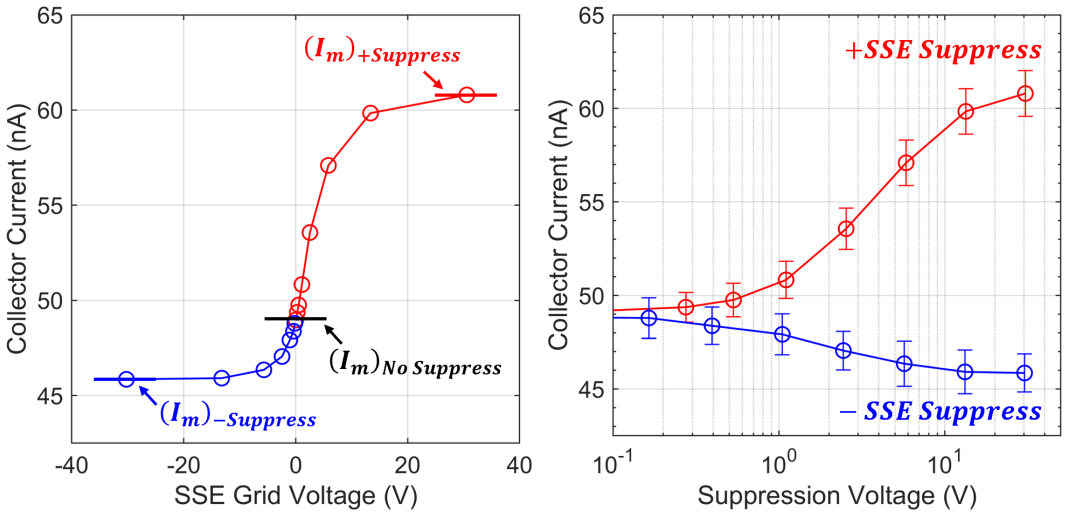


**Fig. 7 (Left) Collector current measured as a function of SSE grid voltage. (Right) That same data plotted with the x-axis on a log scale. Error bars on the right plot show one standard deviation. The "suppression voltage" shown in the right plot is the absolute value of the SSE grid voltage. The charge yields were calculated to be $\gamma^{+}_{SSE} = 0.20$ and $\gamma^{-}_{SSE} = 0.05$. (Nickel collector, ILIS source with EMI-$BF_4$ and $\phi_{Em} = +1.9$ kV).**

The right side of Figure 7 shows the same plot, but with the x-axis on a log scale. The shape of the curves give information about the energy distribution of the secondary species. Note that the error bars shown represent the standard deviation of the measured currents.

### B. SSE-Correction of Time-of-Flight Data

An important practical application for SSE probes is their ability to remove SSE effects from current measurements. That is, they are able to measure the true incident current, $I_P$, without the uncertainty normally introduced by secondary species emission. The importance of this point should not be overlooked—*nearly all* electrospray plume diagnostics rely on the measurement of charged species. All of those diagnostics are subject to errors introduced by SSE effects. In the absence of robust methods to correct these current measurements (e.g., empirical scaling factors), an SSE probe can be used to remove the secondary currents from the measurements. Because the SSE probe is able to differentiate primary current ($I_P$) from secondary currents ($I^{+}_{SSE}$ and $I^{-}_{SSE}$), the secondary species yields do not need to be known beforehand. Rather, the secondary yields are measured for each set of current measurements and used to calculate the primary current, $I_P$.

This section (and the next) will show how an SSE probe can be used in tandem with retarding potential (RP) and time-of-flight (ToF) methods. Figure 8 is a diagram of a tandem SSE / RP / ToF instrument. Surfaces drawn in black are at ground potential. Red denotes electrodes that are held at specified voltages. The RP / ToF instrument used in this study was adapted from Lyne et al. [6, 7] by replacing the current collector (i.e., the ion detector) with an SSE probe. The amplifier responsible for converting the measured current into a voltage signal is located as close as possible to the SSE probe (inside the vacuum chamber) to achieve an acceptable signal-to-noise ratio at the required bandwidth (3 MHz). That is, in order for the amplifier to be "fast enough" and to provide a good-quality signal, the amplifier should be located as close to the collector as possible.

This section discusses how an SSE probe can be used with conventional time-of-flight (i.e., SSE / ToF) to correct for current measurement error due to secondary species emission. Note that the ToF data presented in this section were measured while the RPA voltage was set to $\phi_{RP} = 1820$ V.

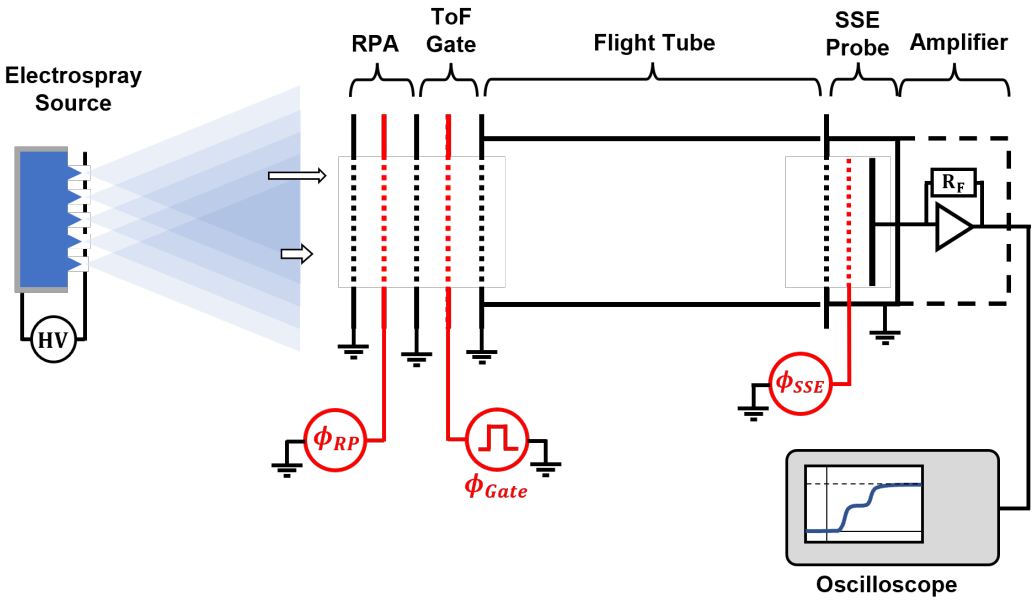


**Fig. 8 SSE probe in tandem with time-of-flight and retarding potential methods, used for measuring the mass spectrum and energy distribution in the plume, respectively.**

Time-of-Flight curves were measured for each of three different SSE suppression conditions, as shown on the left side of Figure 9. The SSE suppression grid potentials were $\phi_{SSE} = [-30\,V, 0\,V, +30\,V]$, corresponding to negative SSE suppression, no suppression, and positive SSE suppression, respectively. Like the DC current measurements in section IV.A, the time-of-flight signal can also be analyzed to find the primary and secondary currents vs. time. The left plot shows the three independent current measurements (one for each suppression conditions), analogous to the measurements in Equations 2, 3, and 4. Using Equations 5, 6, and 7, the primary and secondary currents can be calculated from the measured time-of-flight signals. The right plot shows the results of that calculation, where the true plume current is calculated ($I_P$) as well as both secondary currents ($I^+_{SSE}$ and $I^-_{SSE}$). Thus, $I_P$ is the time-of-flight signal after correcting for SSE effects.

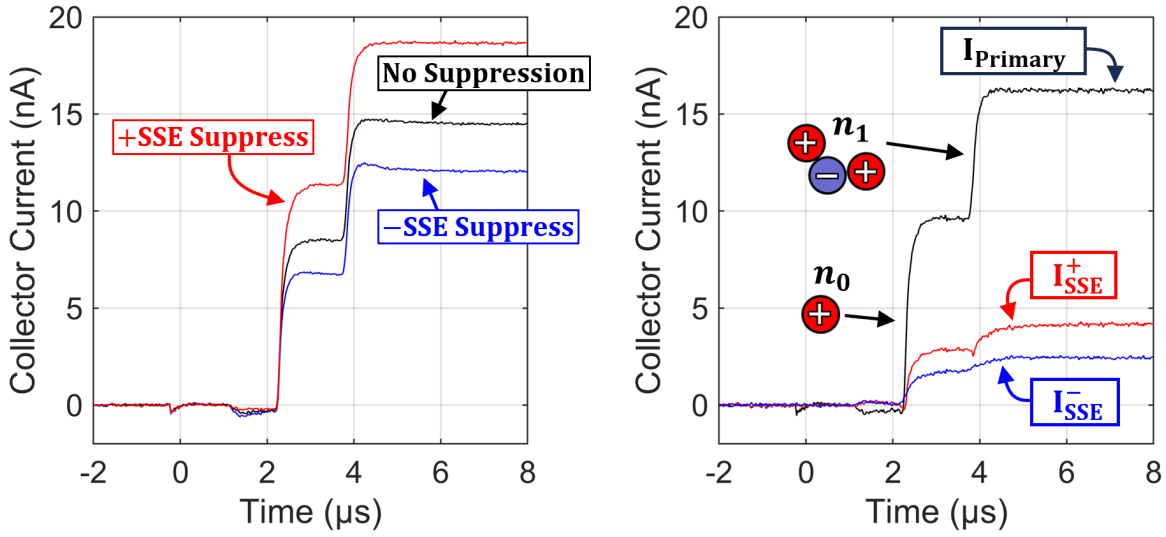


**Fig. 9 (Left) Time-of-Flight curves measured for different SSE suppression conditions. (Right) ToF curves after correcting for SSE effects.**

Figure 10 shows the raw (uncorrected) and corrected time-of-flight curves on the same plot. Note that the 'uncorrected' curve is the ToF data measured with zero SSE suppression and the 'corrected' curve is the primary current, $I_P$, computed from Equation 5. The main difference between the corrected and uncorrected curves is their overall magnitude. The uncorrected ToF data indicate that the plume current density is 10% lower than the corrected value. Analyzing the monomer and dimer fractions in the plume, we find that the corrected and uncorrected curves each imply a monomer ($n_0$) fraction of 59% and a dimer fraction of 41%. The rate of mass flux to the collector surface can be calculated by the product of the plume current and the average mass-to-charge ratio. We find that the standard (uncorrected) ToF data underestimate mass flux by 10%.

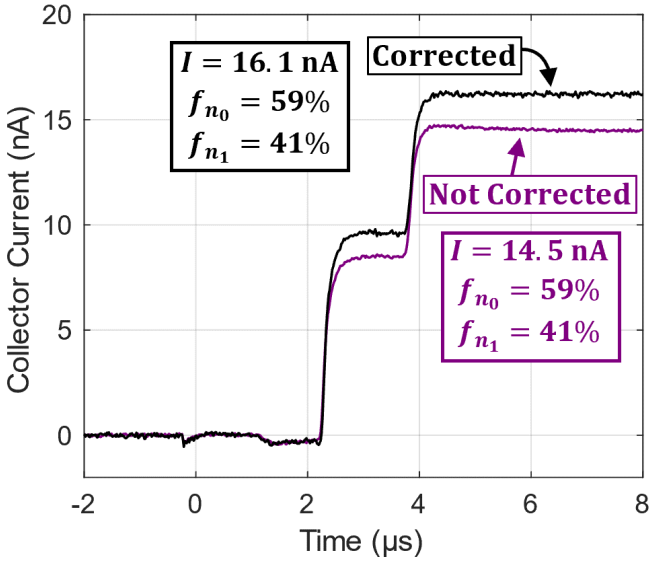


**Fig. 10 Time-of-Flight curve before (purple) and after (black) correcting for SSE effects.**

### C. Measurement of SSE Yields for Specific Species and Energies

A persistent complication in studying electrospray plume-surface interactions is the wide spread of species mass-to-charge and stopping potential values that may coexist within the plume. Molecular dynamics simulations (e.g., [8]) are able to simulate the impact of molecular ions and ion clusters on solid surfaces. However, experimental results for secondary charge yields are often reported as an *average* value for the plume ([1, 2]). Consequently, simulation predictions of electrospray plume-surface interactions are difficult to validate. The SSE probe described in this work can be used in combination with a tandem energy analyzer / mass spectrometer to measure the secondary charge yields for *specific* plume species and *specific* stopping potentials. The instrument shown in Figure 8 shows one way to implement these three methods simultaneously—using a Secondary Species Emission (SSE) probe, Retarding (RP) Potential analyzer, and Time-of-Flight mass spectrometer in tandem. This technique, abbreviated here as SSE / RP / ToF, has two unique capabilities. First, SSE yield can be measured for specific values of $m/q$ and $\phi_{SP}$. Second, the SSE probe can be used to correct ToF and RP / ToF measurements. This may improve the accuracy of ToF and RP / ToF measurements by mitigating errors due to SSE effects, which are difficult to account for and may change as the current collector's surface becomes modified (e.g., sputtering, chemical reactions, deposited material).

Figure 11 shows time-of-flight curves measured for each of six experimental conditions. The solid curves were measured at a retarding potential of $\phi_{RP}$ = 1820 V and the dashed curves were measured with $\phi_{RP}$ = 1772 V. The color of the curve indicates which SSE suppression condition was used—red is +SSE suppress, blue is -SSE suppress, and black indicates that no SSE suppression was used. A figure showing the full dataset is included in the Appendix.

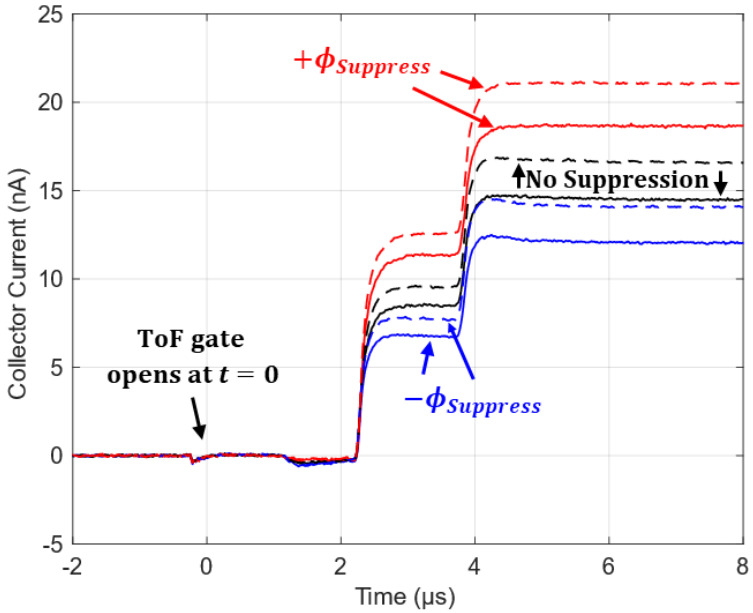


**Fig. 11 SSE / RP / ToF dataset (Figure 14) reduced to six composite time-of-flight curves.**

The ToF signal can be calculated for a specific range of stopping potentials by taking the difference between ToF signals at different RPA voltages, $\phi_1$ and $\phi_2$ (Equation 10). The so-called RP / ToF signal, $y_{(\phi_1<\phi_{SP}<\phi_2)}$, is the ToF curve that corresponds to plume species with stopping potentials (kinetic energies) in the range $\phi_1 < \phi_{SP} < \phi_2$.

$$y_{(\phi_1<\phi_{SP}<\phi_2)} = y_{\phi_1} - y_{\phi_2} \tag{10}$$

For example, the ToF signal at $\phi_{RP} = 1700$ V minus the ToF signal at $\phi_{RP} = 1800$ V yields the ToF signal for species in the range $1700\,V < \phi_{SP} < 1800\,V$. In Figure 11, this is done by subtracting the solid curve from the dashed curve for each color. The resulting curves are shown in Figure 12, which represent the time-of-flight signals associated with plume species with stopping potentials in the range $1772 < \phi_{SP} < 1820\,V$.

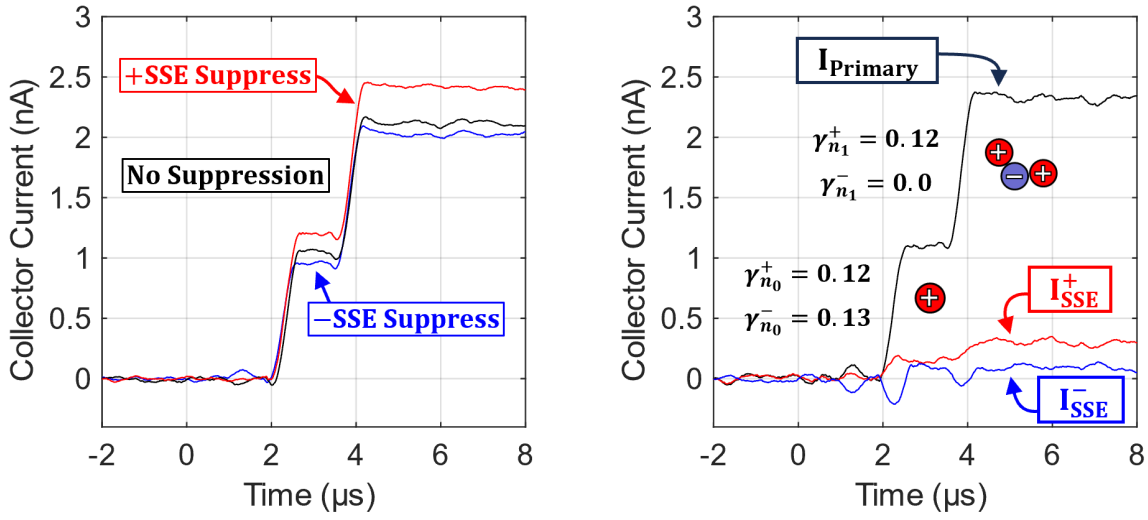


**Fig. 12 (Left) Retarding Potential / Time-of-Flight (RP / ToF) curves measured for three different SSE suppression conditions. (Right) RP / ToF curves after correcting for SSE effects.**

The curves in figure 12 can be analyzed to find the secondary charge yields for specific plume species (i.e., specific $m/q$ values). Single molecular ions, known as monomers and denoted $n_0$, are present in the plume as well as small ion clusters, called dimers and denoted $n_1$. The monomer and dimer signals are clearly separated in figure 12, allowing the signal magnitude ($\Delta I$) to be found. For both species, the signal magnitude was measured for the negative suppression, positive suppression, and no suppression cases. Those measurements—$\Delta I_{-Suppress}$, $\Delta I_{No\ Suppress}$, and $\Delta I_{+Suppress}$ for both monomers and dimers—can be used with equations 2 through 4 to calculate the secondary charge yields for positive EMI-$BF_4$ monomers and dimers at an impact energy of $\phi_{SP} \approx 1800$ V.

Analysis of the RP / ToF curves in figure 12 shows that the signal magnitudes for the monomer step are $\Delta I_{n_0}$ = 472 pA, 540 pA, 606 pA for negative suppression, no suppression, and positive suppression cases, respectively. For dimers, those step magnitudes were $\Delta I_{n_1}$ = 556 pA, 552 pA, 630 pA, respectively. Using equations 8 and 9 to calculate the corresponding yields, we find that the positive and negative secondary charge yields for monomer impact are $\gamma^+_{SSE} = 0.12$ and $\gamma^-_{SSE} = 0.13$. Similarly, we find that the values for dimer impact are $\gamma^+_{SSE} = 0.12$ and $\gamma^-_{SSE} = -0.01$. The negative calculated value for $\gamma^-_{SSE}$ is nonphysical—the analysis approach used here does not allow for charge yields below zero. Rather, it is a consequence of measurement uncertainty. The yield values calculated here are reasonably close to the plume-averaged SSE yield values reported by Klosterman et al. for the same ion source [1]. Furthermore, the values of SSE yield calculated from the SSE / RP / ToF data agree with the plume-averaged yields measured in section IV.A.

Unlike the steady-state SSE measurements in section IV.A and in [1, 2], SSE / RP / ToF measurements are able to resolve the secondary charge yields for *specific* species and *specific* stopping potentials. This method has the potential to provide far more granular data about electrospray plume-surface interactions that are currently available. Perhaps most importantly, the ability of this method to discriminate between the different species and energies in the electrospray plume would allow simulations of single particle impacts to be compared directly to experimental results. That is, one does not need to compute an average SSE yield over all plume species and all plume energies in order to compare to experimental results, greatly reducing the required computational resources.

Figure 13 compares the uncorrected and corrected RP / ToF signals on the same plot, corresponding to the "No Suppression" and "$I_{Primary}$" curves in Figure 12. Like the comparison of corrected vs. uncorrected ToF data (Figure 10), the magnitude of the corrected signal is larger than the uncorrected signal magnitude. The measured plume currents for the corrected and uncorrected cases were 2.3 nA and 2.1 nA, respectively. Thus, we find that plume density implied by the uncorrected data is 9% lower than the corrected case. Another notable feature of Figure 13 is the difference in the dimer fraction. Calculating monomer ($n_0$) and dimer ($n_1$) fractions for each case, we find that the monomer-to-dimer ratio ($f_{n_1}:f_{n_0}$) is 46% : 54% and 52% : 48% for the corrected and uncorrected data, respectively. The average mass-to-charge value calculated from the corrected data is $(m/q)_{avg}$ = 218 amu/q compared to $(m/q)_{avg}$ = 206 amu/q for the uncorrected case (-6% error). We find that the uncorrected RP / ToF data underestimate mass flux to the collector surface by 14% due to the combined errors in plume current and average mass-to-charge.

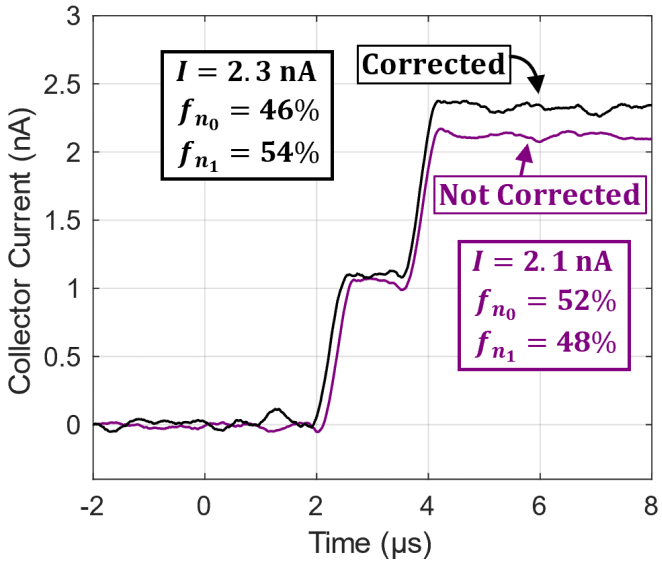


**Fig. 13 Retarding Potential / Time-of-Flight curve before (purple) and after (black) correcting for SSE effects.**

## V. Conclusion

This work investigated the effects of secondary species emission on electrospray plume measurements. We demonstrated, for the first time, how time-of-flight data can be corrected for SSE effects. We show that secondary species emission leads to an underestimation of plume current density by about 10%. Further, measurements using the SSE probe in tandem with energy analysis and mass spectrometry show that the average mass-to-charge ratio can change by 6% when correcting for SSE effects, resulting in an error of 14% for the calculated mass flux.

We demonstrated how SSE correction can be applied to electrospray plume measurements (i.e., time-of-flight, retarding potential / time-of-flight) through two case studies. The first case study demonstrated how time-of-flight data can be corrected for error caused by secondary charge emission from the collector. This capability may be especially useful for capillary plumes, where mass-to-charge can span from 100 amu/q to >100,000 amu/q, thus the range of SSE yields may also vary significantly. For the electrospray source studied here (porous source, $\phi_{Em}$ = +1900 V, EMI-$BF_4$), we found that SSE effects resulted in -10% error in plume current measurements, but had no discernible effect on the average mass-to-charge calculated from the data. The error in mass flux to the collector, which depends on plume current density and average mass-to-charge, was also -10% in this case.

The second case study demonstrated an SSE probe in tandem with retarding potential and time-of-flight methods (i.e., SSE / RP / ToF). Using these three methods in tandem has two primary advantages. First, ToF and RP / ToF data can be corrected for SSE effects. Thus, the characteristics of the plume can be measured more accurately. For the RP / ToF data—ToF curves that represent a narrow range of species energies—SSE effects resulted in -9% error in measured plume current and -6% in average mass-to-charge, resulting in -14% error in mass flux to the collector. The second advantage of SSE / RP / ToF is the unique capability to measure SSE yields for *specific* species at *specific* energies. The resulting data is considerably easier to use for model validation than the SSE data that are currently available in the literature, which report an average SSE yield for all species and energies in the plume. We expect SSE / RP / ToF to be an important experimental method to support the development and validation of electrospray plume-surface interaction models going forward.

## Appendix

Figure 14 shows the full oscilloscope record (i.e. the full dataset) for the SSE / RP / ToF measurements presented in section IV.C. The record contains one hundred time-of-flight “events", each of which consists of an open / close cycle of the ToF gate and the corresponding collector current vs. time ($I_c = f(t)$). The record contains ToF curves for six different experimental conditions, one for each combination of $\phi_{suppress} = -30\,V, 0\,V, +30\,V$ and $\phi_{RP} = \phi_1, \phi_2$. ToF curves for each experimental condition were synchronized and averaged to yield a single representative ToF curve for

that combination of SSE suppression voltage ($\phi_{suppress}$) and RPA voltage ($\phi_{RP}$). Those six representative curves are shown in Figure 11.

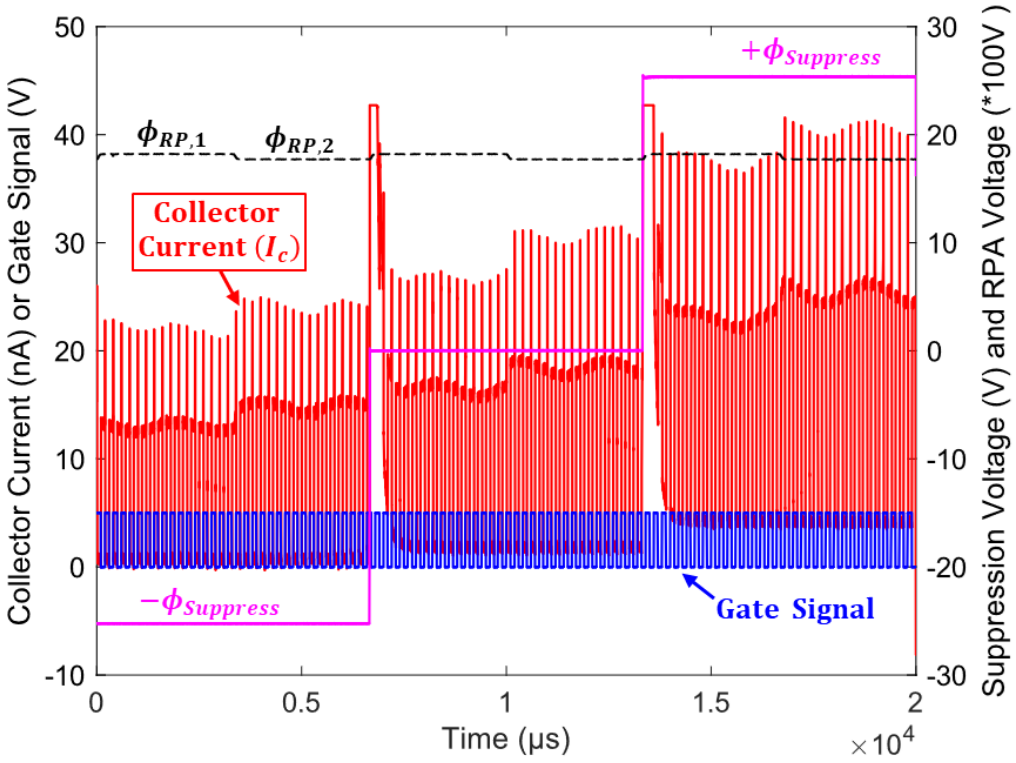


**Fig. 14 SSE / RP / ToF dataset, which contains one hundred Time-of-Flight "events". Those 100 ToF curves were divided into six experimental conditions: -SSE Suppress, No Suppression, and +SSE Suppress for two different RPA voltages. ToF curves from within each region were synchronized and averaged to improve signal-to-noise ratio.**

## References


[1] Klosterman, M. R., Rovey, J. L., Levin, D. A., and Rao, A., "Ion-induced charge emission from unpolished surfaces bombarded by an [Emim][BF4] electrospray plume," *Journal of Applied Physics*, Vol. 131, No. 24, 2022. https://doi.org/10.1063/5.0060615, URL https://doi.org/10.1063/5.0119297.

[2] Uchizono, N. M., Wirz, R. E., Collins, A. L., Marrese-Reading, C., Arestie, S. M., and Ziemer, J. K., "A diagnostic for quantifying secondary species emission from electrospray devices," *Review of Scientific Instruments*, Vol. 94, No. 2, 2023, p. 025008. https://doi.org/10.1063/5.0117666, URL https://doi.org/10.1063/5.0117666.

[3] Uchizono, N. M., Wright, P. L., Collins, A. L., and Wirz, R. E., "Emission spectra of glows produced by ionic liquid ion sources," *Applied Physics Letters*, Vol. 121, No. 15, 2022, p. 154101. https://doi.org/10.1063/5.0096595, URL https://doi.org/10.1063/5.0096595.

[4] Uchizono, N. M., Collins, A. L., Marrese-Reading, C., Arestie, S. M., Ziemer, J. K., and Wirz, R. E., "The role of secondary species emission in vacuum facility effects for electrospray thrusters," *Journal of Applied Physics*, Vol. 130, No. 14, 2021. https://doi.org/10.1063/5.0063476, URL https://doi.org/10.1063/5.0063476.

[5] Adduci, A., "Characterization of a multimode propellant operating in a porous glass electrospray thruster," Master's thesis, University of Illinois Urbana-Champaign, 5 2023.

[6] Lyne, C. T., Liu, M. F., and Rovey, J. L., "A simple retarding-potential time-of-flight mass spectrometer for electrospray propulsion diagnostics," *Journal of Electric Propulsion*, Vol. 2, No. 1, 2023, p. 13. https://doi.org/10.1007/s44205-023-00045-y, URL https://doi.org/10.1007/s44205-023-00045-y.

[7] Lyne, C. T., Liu, M. F., and Rovey, J. L., "A Low-Cost Linear Time-of-Flight Mass Spectrometer for Electrospray Propulsion Diagnostics," *37th International Electric Propulsion Conference*, Cambridge, MA, 2022, pp. 2022–178.

[8] Bendimerad, R., and Petro, E., "Molecular dynamics studies of ionic liquid-surface interactions for electrospray thrusters," *Journal of Electric Propulsion*, Vol. 1, No. 1, 2022, p. 27. https://doi.org/10.1007/s44205-022-00032-9, URL https://doi.org/10.1007/s44205-022-00032-9.